CrossMark

ORIGINAL ARTICLE

Microstructural morphology and evolution of austenite stainless steel deposited using pulsed laser and wire

Jiang-zhou Su[1] · Mu-zheng Xiao[1] · Zhi-jing Zhang[1] · Zhi-peng Ye[1] · Xin Jin[1] ·
Yi-chong Yang[1]

Abstract A deposition process based on pulsed laser processing and wire feeding was employed in this study to fabricate high-performance components. The microstructural morphology and evolution of SUS304 austenite stainless steel were examined in detail. The thin wall and ladder block samples, considered as two representative structures of metal additive manufacturing, were deposited. It was found that the microstructure is homogeneous in all the deposited samples. For the thin wall, columnar grains, which are normal to the substrate with a growth tendency to the surface and scanning direction, dominate the deposition. Columnar grains along the cooling gradient and equiaxed grains are both observed in the surface. These different grain morphologies result in different microhardness values, and the microhardness in pulsed laser deposition is universally higher than that in a 304 cold rolling metal substrate. For the ladder block, columnar grains are observed along various directions. Further, it is found that the variation in the shape of the molten pools is an essential reason for the evolution of the microstructures with the addition of the deposited layers. It not only change the nucleation condition and cooling directions near the boundaries in the molten pools, but also leads to a recrystallization along the new cooling directions in the heat-affected zone.

Keywords Pulsed laser · Wire feed deposition ·
Microstructural morphology · Microstructural evolution

✉ Mu-zheng Xiao
muzheng_xiao@bit.edu.cn

✉ Zhi-jing Zhang
zhzhj@bit.edu.cn

[1] Laboratory of Micro Manufacture Technology, School of Mechanical Engineering, Beijing Institute of Technology, Beijing 100081, China

1 Introduction

Metal additive manufacturing (AM) technology, which involves fabricating components by depositing raw metallic materials via a predetermined path, has received tremendous attention in recent years. Research studies indicate that AM technology has the potential for rapidly prototyping metallic components with lower cost and higher efficiency compared to traditional manufacturing methods [1, 2].

Currently, various methods are being proposed for achieving metal AM with different forms of raw materials or energy sources. Using metal powders as raw materials in spraying powder-based processes and powder bed-based processes for metal AM is of more concern to researchers. Although powder-based processes have enabled the successful fabrication of some engineering components in commercial applications [3, 4], they also have some associated problems. The utilization of metal powder is limited, and the quantity of metal powder strongly affects the quantity of deposition [4, 5]. In particular, for powder bed-based processes, the porosity defect caused by unmelted metal powder always remains in the deposited parts. Consequently, powder bed system is restricted to fabricating fully dense parts directly [6–8]. Some post treatment techniques have been proposed for enhancing the mechanical properties of powder-based metal AM components. Previous studies have proven that post heat treatment such as hot isostatic pressing (HIP) effectively reduces the porosity during deposition and improves fatigue strength of the components fabricated by powder-based metal AM [9–11]. However, post treatment is limited in its ability for eliminating high porosities or the tunnel defect that breaches the surface [12].

A metal wire-based deposition process offers significant advantages of low cost, high utilization of raw material, etc. [13]. Several types of metal wires have been researched

including wires of titanium alloy [14–17], nickel-based high temperature alloy [18–20], and iron-based alloy [21, 22]. Generation of metal wires is much easier than that of metal powders, and the wire feed control is a mature process owing to its related applications in the field of welding. Researchers at NASA Langley research center reported a high deposition rate of 2500 cm^3/h for bulk metal deposition under electron beam freeform fabrication (EBF^3) process by metal wire of different materials, including aluminum and titanium alloy [23]. Nie et al. used the laser hot wire (LHW) process for depositing an H13 steel wire at a rate of 3.46 kg/h (441 cm^3/h) using a laser beam with a power of less than 10 kW, which showed the possibility of depositing a metal efficiently via a wire-based process [22]. Because a complete densified component can be deposited by the wire-based process, it has the potential for fabricating components with high mechanical properties in a single step. Nonetheless, significant investigations need to be further performed with regard to the wire-based process for the purpose of attaining a non-defect deposition with good microstructures [14–22].

It is known that microstructures play a decisive role in the mechanical properties of the deposited material regardless of the influence of defects. Previous studies have suggested that microstructures formed under different types of energy sources are similar for the same metallic material. It is found that coarse columnar grains, which grow epitaxially from the substrate, always dominate in the deposition [14–22]. The large amount of heat accumulation during a continuous heat input lead to a significant residual stress, which makes the deposition prone to cracking. On this basis, although the tensile strength comparable to that of cast or forged parts has been obtained in some AM processes [24], the fatigue properties and qualified rate of metal AM parts are still difficult to match the industrial demand [25].

In general, finer microstructures are formed under a faster cooling rate, and the grain growth direction is always along the cooling direction. The relationship between the cooling rate and the microstructure of the deposits has been demonstrated by previous studies. Researchers can control the cooling rate by using different external cooling devices or by applying different deposition parameters [26, 27]. In one case, the terminating microstructure morphology obtained by different deposition processes was observed for evaluating the characteristics of the deposition via a specific process. In the other case, the evolution of microstructures was studied for acquiring the cooling history of a deposition process, based on which a general methodology for controlling the local microstructure can be further proposed. Furthermore, the energy input directly impacts the thermal history of molten pools and depositions. In a traditional metal AM process, the energy source is always continuous, which results in the continuous heating of the depositions. Consequently, inhomogeneous microstructures will form in the depositions, under different

cooling conditions, in each layer of the deposition owing to heat accumulation [15, 16].

A pulsed energy process has the characteristics of shorter heating time and higher instantaneous power compared to continuous energy for the same overall power input. Pulsed energy has been widely used in thin plate welding because of the low thermal shock to the metallic material [28, 29]. In the field of metal AM, some researches using pulsed laser or arc as the energy source have also been reported [30–32]. In particular, Nassar et al. compared the difference between a continuous laser input and a pulsed laser input in a spraying powder-based process. They found that the pulsed laser deposition of TC4 showed homogeneous microstructures as well as indentation hardness with deposition height while the continuous laser deposition of TC4 showed a statistically significant decrease in hardness and an increase in lath width near the middle of the deposition [33]. Morgan et al. used a pulsed laser for depositing 316-L stainless steel in a powder bed-based process. The deposition had no unmolten metal powder and the residual stress on the deposition was significantly decreased [31]. Generally, the pulse parameters (pulsed width/frequency) of a pulsed energy input process significantly influence the resulting deposition. If the energy of each pulse is very low, the metal will be unable to melt. If the energy of each pulse is very high, excessive vaporization of the metal and plasma will occur, which will restrain the absorption of energy.

To fabricate components with good mechanical properties and at a low cost, our research group developed a hybrid machining tool based on additive and subtractive processes, of which the additive process used a pulsed laser and wire feeding [34]. A series of preliminary studies were performed for the pulsed laser-based deposition process with a metal wire. In this work, the morphology and evolution of the microstructure in SUS304 austenite stainless steel depositions are further studied. According to the structures that commonly exist in additive manufacturing components, the thin wall and ladder block structures were deposited as two types of samples in this investigation. All the deposited samples are observed in two orthogonal sections.

2 Experimental procedure

2.1 Methodology of pulsed laser deposition with metal wire

2.1.1 Experimental setup

A hybrid machining device based on laser deposition and milling was employed in this study. The overall structure of the device is shown in Fig. 1 and the part involved in laser deposition is marked with dashed lines. The laser beam is
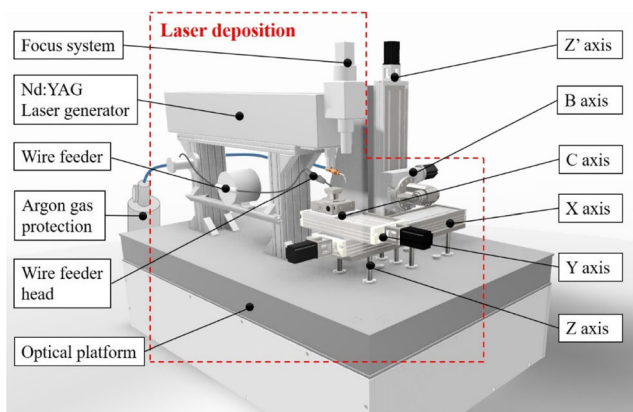
Fig. 1 Overall structure of the hybrid machining device that includes the laser deposition function marked by a *dashed line* [34]

produced by a Nd:YAG laser generator of 1.06-μm wavelength. The deposition process is under the protection environment of Ar gas.

2.1.2 Material

The metal substrate and wire used in this study were both composed of SUS304 stainless steel. The diameter of the metal wire was 0.6 mm. The chemical composition of SUS304 is provided in Table 1. The substrate was an industrial cold rolling plate. Before the experiment, the surface of the substrate was polished and cleaned with acetone and alcohol to remove impurities such as oil stains and surface oxide.

2.1.3 Deposition process of samples

The thin wall and ladder block structures, which are considered as representative structures in metal AM, were deposited as the samples in this study. The parameters used in this study were based on the previously reported preliminary investigation of our research group [34].

Figure 2 illustrates the method of energy input and wire feed. The input current (I) for the laser generator is a square wave of 300 A. The pulse repetition frequency is 3 Hz with 4 ms as the width of the pulse (Fig. 2a). The average energy of single-shot pulsed laser measured with a commercial joulemeter is 38 J. Based on our experience, using a negative defocus laser beam as an energy source is a better method for attaining a smooth side surface. The smoothening of the side surface is a result of the action of gravity and surface tension
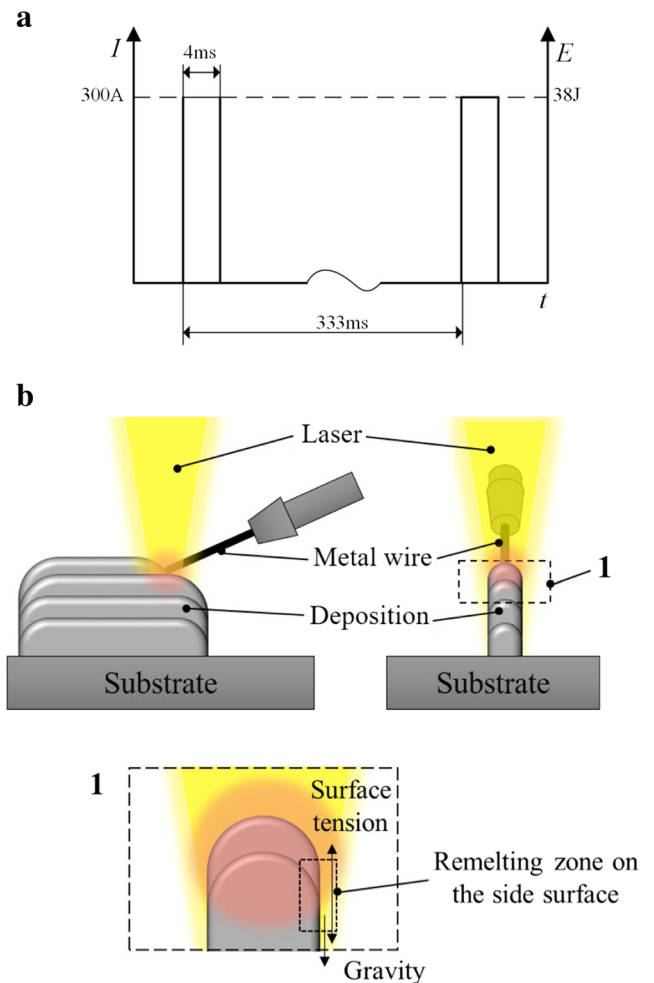

Fig. 2 Energy input and wire feed method: **a** Wave of current input and **b** positions of the laser and wire feed. In **a**, 300 A is the input current, 4 ms is the width of the pulse, 333 ms is the interval time between the two adjacent input current according to the frequency of 3 Hz, and 38 J is the average energy of single-shot pulsed laser. **b** Position *1* shows the action of gravity and surface tension owing to the remelting on the side of the deposition under the negative defocused laser beam

owing to the remelting on the side of the deposition under the negative defocused laser beam (Fig. 2b).

Figure 3 shows the scanning strategy of the thin-wall structure, in which the deposition directions are indicated by arrows. Eight different thin-wall samples were deposited with 1, 2, 3, 5, 8, 13, 21, and 34 layers, which are referred to as S1, S2, S3, S5, S8, S13, S21, and S34, respectively. The processing parameters for the thin wall sample are recorded in Table 2. Moving distance of the Z-axis in each layer in S1–S34 samples is recorded in Table 3. In this study, the shapes of molten pools vary with the deposition process. Therefore, the increase in height of depositions are different in each layer of depositions, which will be lower in the first few layers and be stable after nine layers of the depositions, as shown in Table 3.
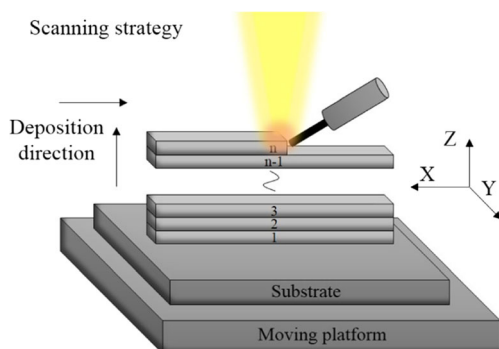
Table 1 Components of 304 stainless steel used in this work (wt%)

C	Si	Mn	Cr	Ni	S	P	Fe
≤0.08	≤1.0	≤2.0	18.0–20.0	8.0–10.0	≤0.03	≤0.05	Bal

Fig. 3 Scanning strategy of the thin-wall structure. The deposition directions are indicated by *arrows*

Figure 4 shows the scanning strategy of the ladder block structure. The processing parameters for the ladder block were the same as those for the thin wall, as listed in Table 2. Six different ladder block samples were deposited with 1, 2, 3, 5, 8, and 13 layers, which are represented as X1, X2, X3, X5, X8, and X13, respectively. The scanning path is always along the same direction from the beginning of each layer, as depicted in Fig. 4a, in which the deposition directions are indicated as arrows. The overlap ratio for each adjacent bead is 0.5, and the beads in a particular layer are always deposited exactly over the corresponding beads of the previous layer, as shown in Fig. 4b. Herein, the "overlap ratio" is recorded as OV_r, and calculated using Eq. 1:

$$OV_r = OL/W \qquad (1)$$

where OL is overlap width and W is single bead width, as shown in Fig. 4b.

Furthermore, for recording the temperature history of the molten pool in the deposition process, infrared thermography was applied. The corresponding method is illustrated in Fig. 5. The FLIR X6530sc was the infrared thermo-graph used in this study.

2.2 Observation process of microstructures

Figure 6 shows the different sections for metallographic observation, which are represented as sections X and Y. Section X is normal to the scanning direction, while section Y is parallel to the scanning direction. All the cross-sections were made by wire cutting. The metallographic samples were mounted, ground, and polished. The sample sections were electrically etched by 10% oxalic acid and 3–4 V electrolysis voltage for

about 30 s. Microstructures were observed by an ordinary optical microscope and a laser confocal microscope. The OLS4100 OLYMPUS was used as the laser scanning confocal microscope in this study.

3 Experimental result

3.1 Microstructures of thin wall samples

The macro appearance of section X in the thin-wall samples is shown in Fig. 7 (contours of the molten pool in the top layer are outlined, which are discussed subsequently). The microstructures in sections X and Y are observed for all the samples, but only typical results are displayed in this paper. Since the microstructural morphology is mainly combined with directional columnar grains, it is described by both grain growth directions and grain size. The different grain growth directions on local positions will cause the anisotropy of depositions, which will influence both the integral and local mechanical properties.

3.1.1 Microstructural morphology

With a rapid solidification process, the internal microstructure is homogeneous with fine columnar dendrites in the thin wall samples. Only primary dendrites are observed. The microstructure morphology is similar in each thin wall sample, and the microstructure of substrate consists of typical equiaxed austenite grains with few twin grains.

Figure 8 presents the microstructures at different positions in section X of sample S34. Because the cooling rate is extremely fast and no subsequent remelting or heat accumulation occurs in the substrate. It is found that the boundary between the deposition and substrate is extremely clear. Fine vertical columnar grains grow along the fusion lines and no obvious heat-affected zone (HAZ) is present (Fig. 8, position 5).

All the middle positions are composed of fine columnar grains with strong directionality (Fig. 8, positions 2–4, the arrows show the grain-growth directions). The width of the austenite columnar grains is only about 1.5 μm and it is constant in these positions. On the contrary, in a typical continuous energy input deposition, an inhomogeneous microstructure always appears with a few differently sized coarse columnar grains in the multiple layers [14–22]. Wang et al. and

Table 2 Processing parameters for deposition of thin-wall sample

Parameter	Energy of single-shot pulsed laser	Laser input current	Width of pulse	Repetition frequency	Wire feeding speed	Scanning velocity	Defocusing distance
Value	38 J	300 A	4 ms	3 Hz	4 mm/s	25 mm/min	−10 mm

Table 3 Moving distance of Z-axis in each layer (mm)

	1st–5th layer	6th–8th layer	≥9th layer
S1–S34	0.1	0.2	0.3

Nassar et al. had obtained similar results about the stability of the internal microstructure of a titanium alloy under a pulsed energy input, which might be a special microstructural characteristic of pulsed energy-based deposition [15, 33].

On the top and side surfaces, a particularly fine-grain region appears, whose thickness is about 20 μm on the top surface and 10 μm on the side surface (Fig. 8; positions 1, 6, and 7). The grains in these areas have a "cellular shape." It is known that nucleation always begins at the bottom of the molten pool and the grain grows along the normal direction of the fusion line. Furthermore, when the solidification reaches the surface of the molten pool, the liquid metal is left to a small region on the surface, which implies that the temperature gradient is strongly reduced in this region. Consequently, production of equiaxed grains on the surface is induced.

At the bottom of each molten pool, a special relatively coarse columnar grain region emerges (Fig. 8, position 6). The width of the coarse columnar grains is about 3 μm in

section X. This region is particularly clear on the top of the deposition, particularly in the side position (Fig. 8, position 8). In the deposition process with continuous energy input, a "layer band" always exhibits with different grain morphology between adjacent layers, which is caused by the remelting of previous deposition [35–37]. When the pulsed energy input is applied, each pulse energy will cause a remelting of the previous deposition. The production of coarse grains indicates a slower cooling rate in the remelting region near the fusion lines, especially for the side position.

Figure 9 shows the typical microstructure in section Y of the thin wall samples, which exhibits a similar variation about the grain growth in the deposition direction of each layer. In each individual deposited layer, the columnar grain-growth direction varies significantly in section Y, which can be explained by the different grain-growth directions in different positions of the single molten pool (Fig. 9, position 1, the arrows indicate the grain growth directions). The columnar grain always points to the scanning direction and grows along the normal direction of the fusion line in each molten pool. Consequently, the length direction of the columnar grain becomes horizontal gradually from bottom to top in the same deposited layer. In particular, the fine grain found in the top surface is a mixture of equiaxed grains and columnar grains along the scanning directions as depicted in position 2 of Fig. 9. When the columnar grains are almost parallel to the scanning direction, the cellular shape grains appear in section X. The diameter of equiaxed grains and the width of columnar grains in the surface of the deposition are less than 1 μm, which are finer than the columnar grains in the middle positions.
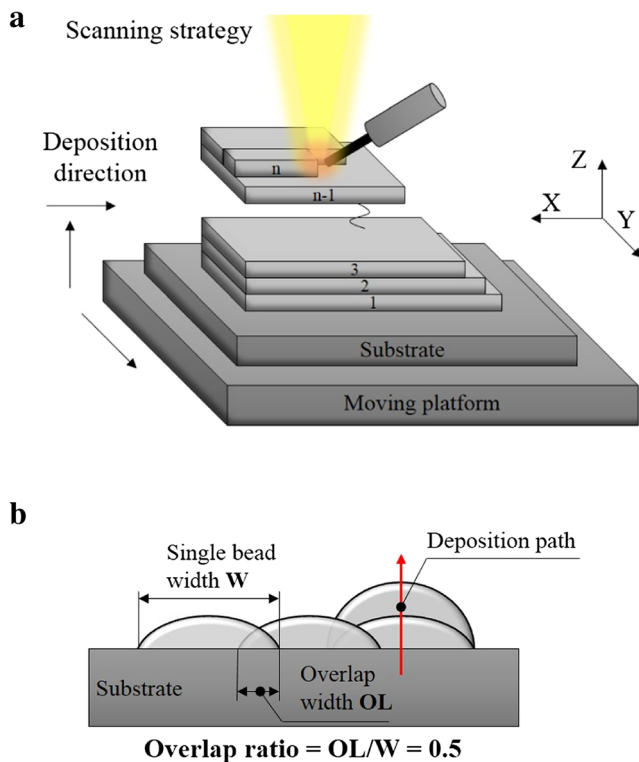

Fig. 4 Scanning strategy of the ladder block structure: **a** scanning strategy and **b** sketch of overlap and deposition path. **a** The deposition directions are indicated as *arrows*. **b** The deposition path of the beads in a particular layer is indicated by a *red arrow* on the *right side*
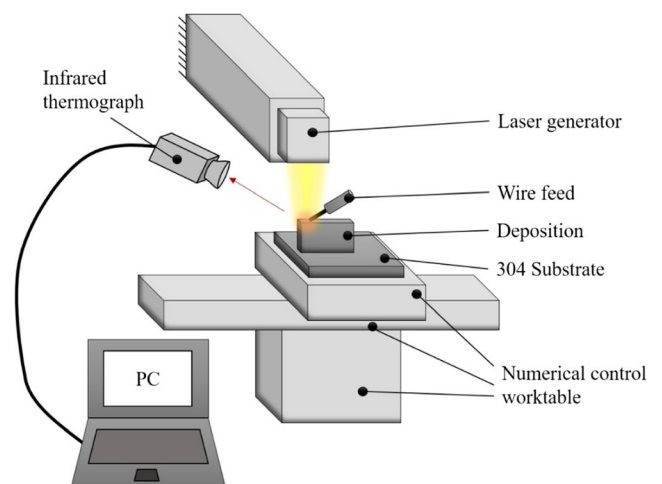

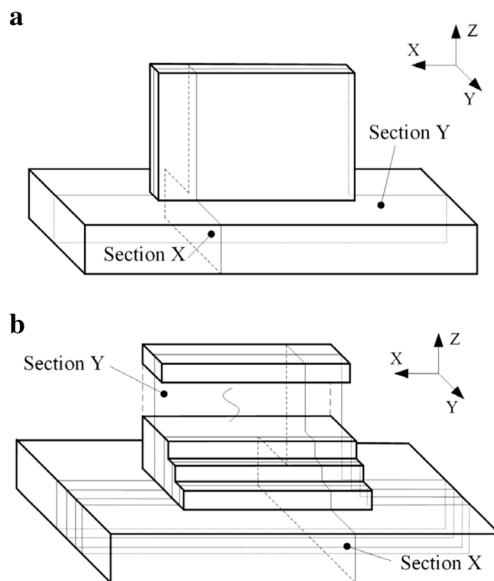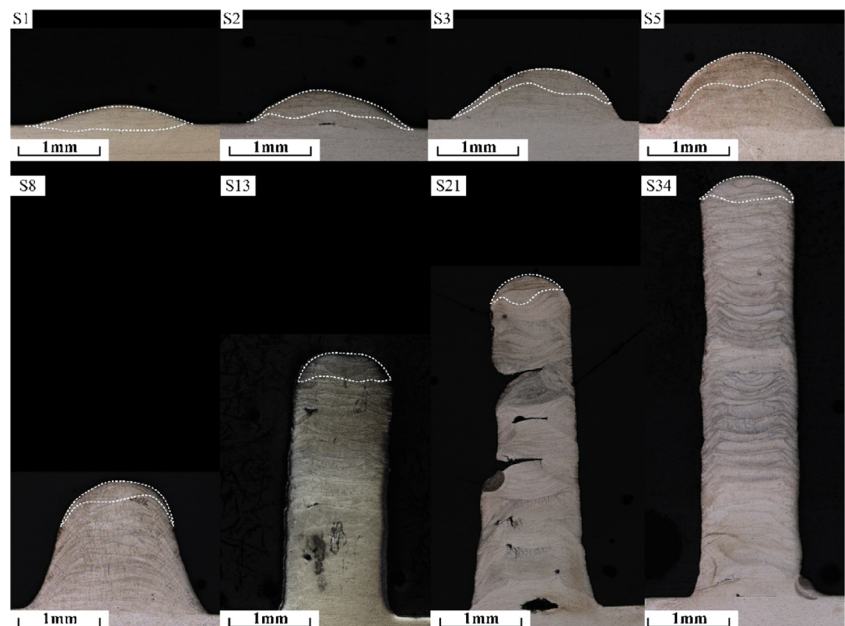**Fig. 5** Schematic of the method for recording thermal history

Fig. 6 Sections for metallographic observation in **a** thin wall and **b** ladder block. Section *X* is normal to the scanning direction, while section *Y* is parallel to the scanning direction

3.1.2 Microstructural evolution

Figure 10 shows the tendency of grain-growth at the same position in section *X* of different thin wall samples. The growth direction of the columnar grains is traced in each picture. Although the same position is compared, different grain morphologies are observed for different samples because of the effects of reheating and remelting (Fig. 10a). The grain growth direction in the remelting zone and the grain morphology in the previous deposition are both changed (Fig. 10b). In the beginning of the deposition process, the grain

growth direction is vertical and points to the center of the top surface. With the increase of deposited layers, the top surface remelts and new microstructure morphology is formed. The direction of grain growth tends to gradually become epitaxial. The grain growth direction becomes stable after a 13-layer deposition.

3.2 Microstructures of ladder block samples

Because the directions of grain morphology in the ladder block samples is more complicated, different positions in both sections *X* and section *Y* are synthesized for explaining the three-dimensional morphology of the grains at different positions.

3.2.1 Microstructural morphology

The microstructures of sections *X* and *Y* in the ladder block sample X13 are shown in Figs. 11 and 12, respectively. The top surface of the ladder block has a chaotic grain morphology (Fig. 11, position 1). Various grain morphologies are formed on the surface of section *X*, which may be a result of columnar grains with different directions synthetically considered with section *Y*.

It is found that vertical columnar grains dominate in both sections *X* and *Y*, and the length direction of the columnar grain gradually becomes horizontal from bottom to top in the same deposited layer, which is similar to the thin wall case (Fig. 12, position 2). Additionally, for the ladder block, each deposited bead is based on both an adjacent bead and previous depositions. Therefore, compared to the thin wall samples, shapes
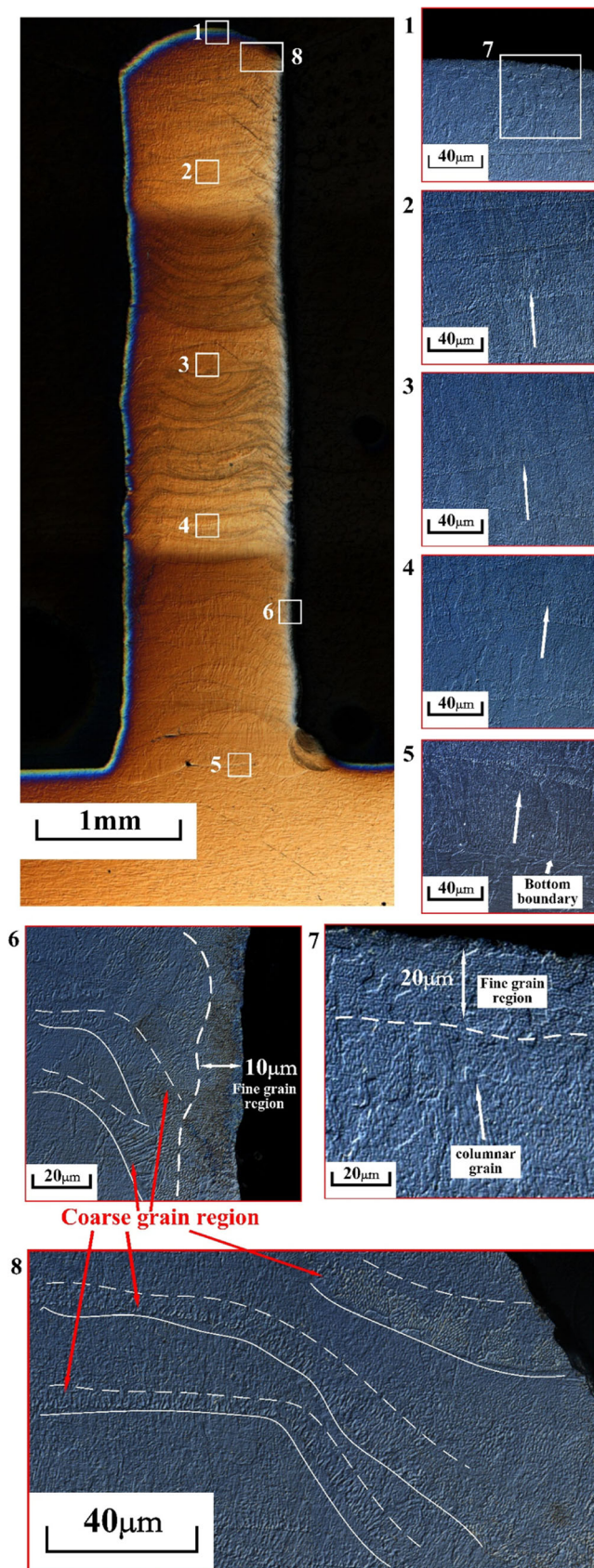
Fig. 7 Appearance of section *X* of thin wall samples with different layers

Fig. 8 Microstructures at different positions in section *X* for sample S34. *2–5* The *arrows* represent the grain-growth directions

of the molten pools in the ladder block samples are asymmetrical, which result in different cooling directions and surface tension directions. Consequently, the microstructures are more complicated at all positions of the ladder block structures. Several different morphology grains are found within the fusion lines of the molten pool (positions 1 and 2 in both Figs. 11 and 12, referred to as the "special grain region"). This special grain region has a macroscopic "triangular shape."

Moreover, it is found that the bottom boundary of the ladder block is unclear with several interlaced fusion lines because of the overlap process. The coarse
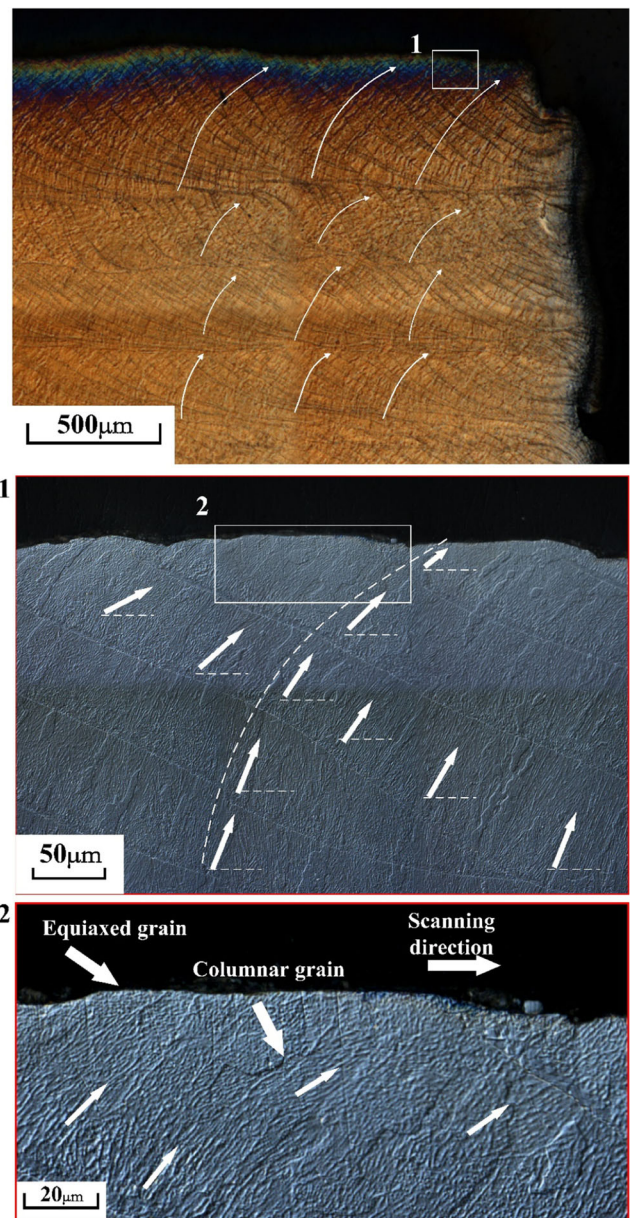

Fig. 9 Typical microstructure in top surface of section *Y* of the thin wall samples. The *arrows* indicate the grain growth directions

Fig. 10 Evolution of grain growth direction in the thin wall samples: **a** grain morphology at the same position in different thin wall samples and **b** variation of grain-growth. **a, b** The *solid lines* indicates the terminal grain morphology. **a** The horizontal axis shows the thin wall samples of S1–S34 and the *vertical axis* shows the different positions in the deposition direction. **b** The *dashed lines* indicate the previous grain morphology, and the *arrows* indicate the variation of grain morphology
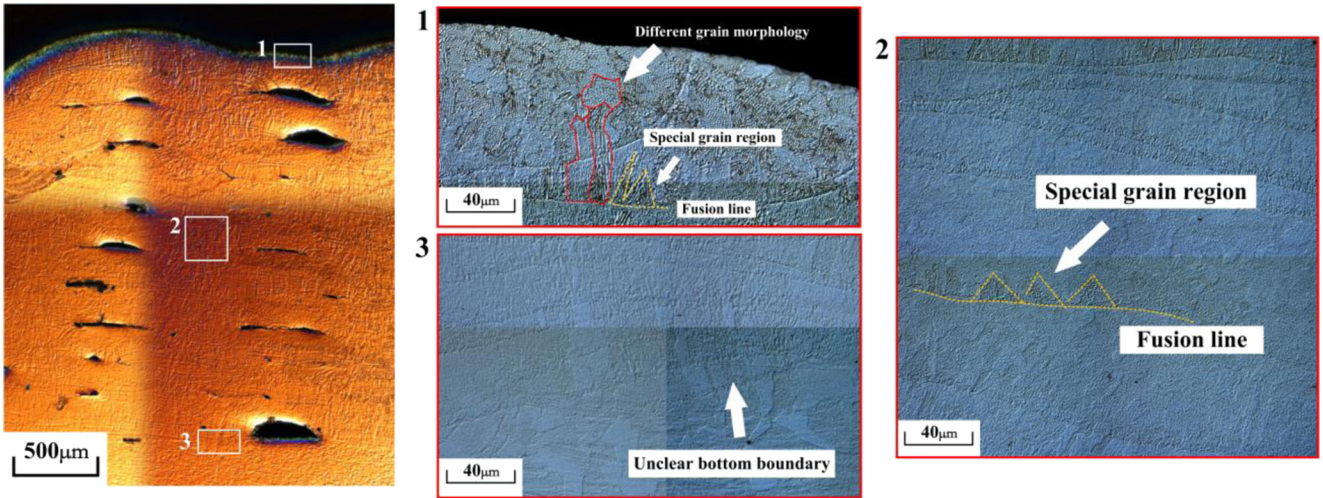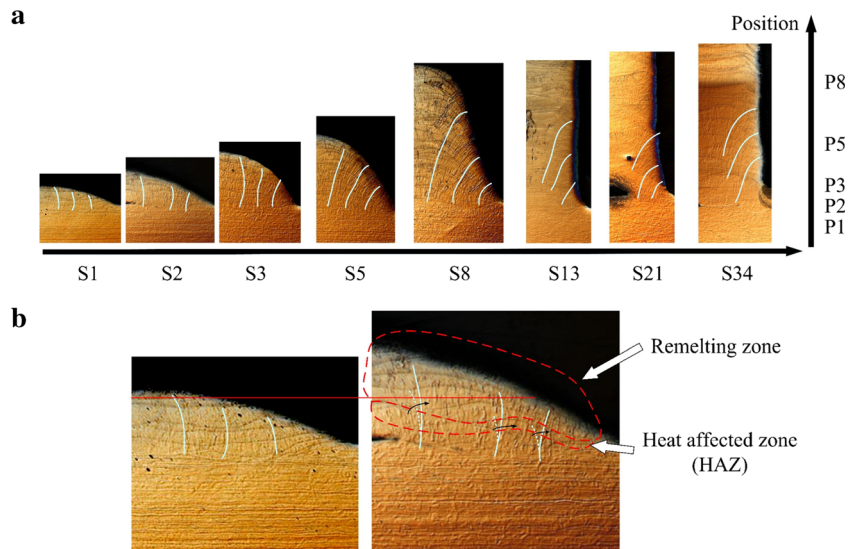

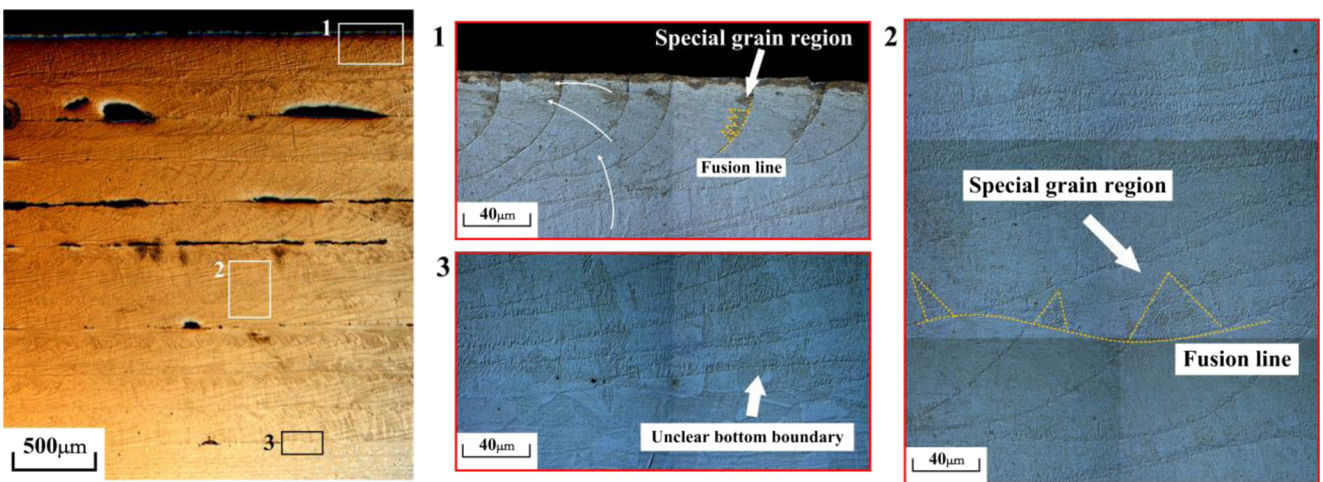**Fig. 11** Microstructures observed in section *X* of ladder block sample X13

Fig. 12 Microstructures observed in section *Y* of ladder block sample X13
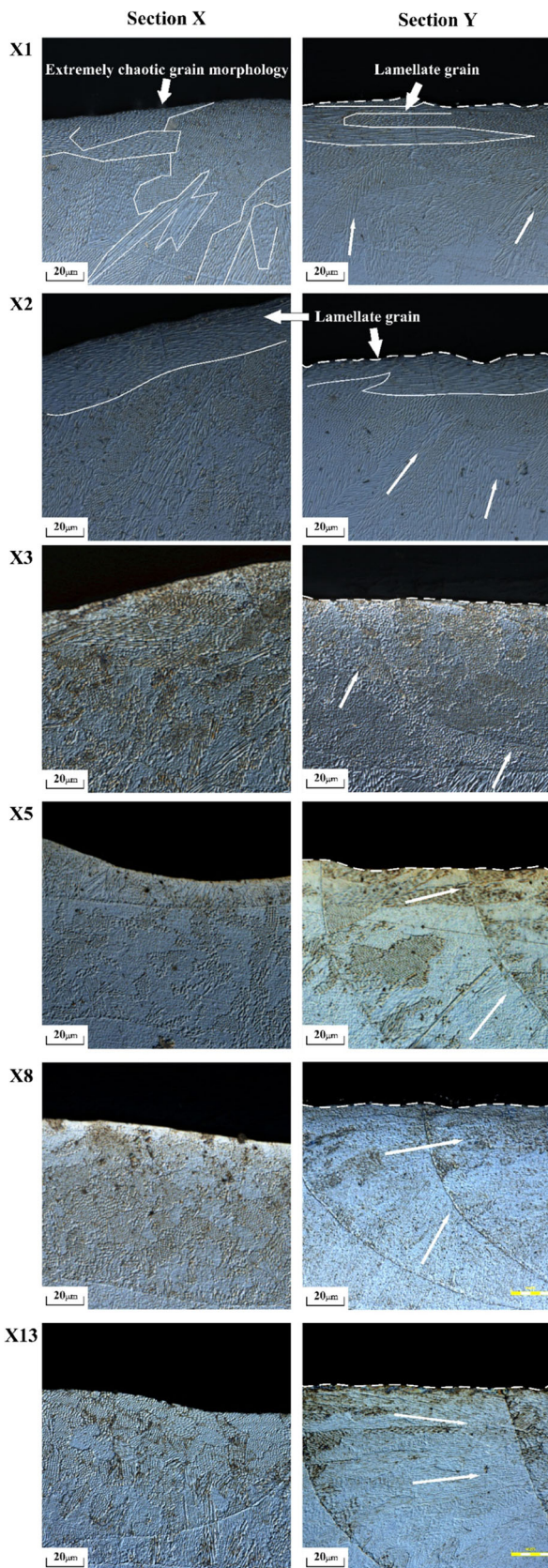
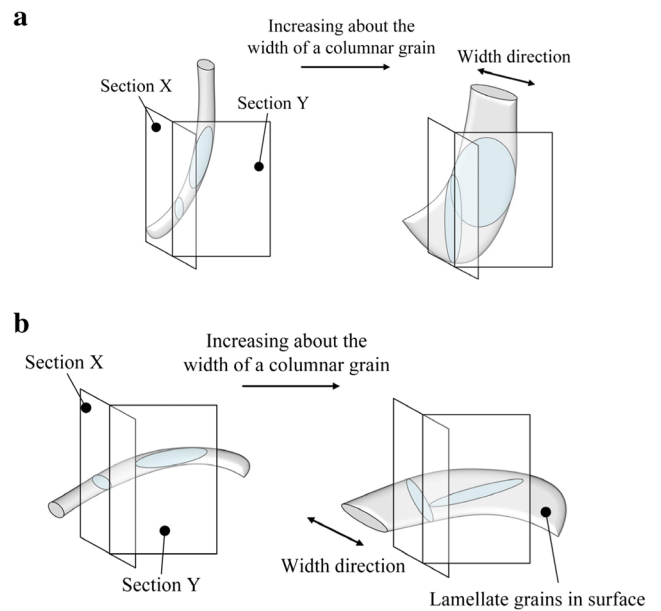Fig. 13 Microstructures in the top position of sections *X* and *Y* of each of the ladder-block samples

Fig. 14 Grain shapes observed in sections *X* and *Y* for different grain morphologies: **a** vertical grain and **b** horizontal grain

austenite equiaxed grains of substrate is not completely melted, and the columnar grains are recrystallized inside these coarse equiaxed grains in this area (Figs. 11 and 12, position 3).

3.2.2 Microstructural evolution

Microstructural evolution is also observed for ladder block deposition. Generally, the deposition process for ladder block samples is more stable because the multiple beads in each layer lead to a smooth surface for the previous layer in the next layer deposition process. Therefore, the variation of the microstructure at the same position of different ladder-block samples is not obvious.

However, the microstructures on the top surface of different samples are clearly changed, particularly for samples X1–X3. Figure 13 shows both sections *X* and *Y* of the ladder block samples with different deposited layers. It is found that the top profile of section *Y* in X1 and X2 is quite uneven, and a clear fluctuation is observed even in a single molten pool, which indicates the deposition process in this position is unstable. The grain morphology near the top surface is extremely chaotic in the first two deposited layers. Figure 14 displays that grain shapes are formed in sections *X* and *Y* for different grain morphologies. Comprehensively considering the two-section microstructural pictures, it is found that several grain shapes are produced at these positions. The chaotic microstructure morphology can be

explained in terms of the increase of the width of co-lumnar grains (Fig. 14a) and the versatile directions of the columnar grains. When the width of the columnar grains is large enough, lamellar grains are formed (Fig. 14b), a feature that is observed in case of deposition of 1–2 layers. With the additive process of ladder block, the chaotic extent of grains near the surface decreases gradually, and the grains on the surface instead become more directional with the deposition process. The fine columnar grains that point to the scanning direction dominate the surface finally.

3.3 Defects

The internal defects of the pulsed-laser deposition with metal wire include incomplete fusion, cracking, and porosity. Figure 15 displays the typical incomplete fusion defects, which are considered to be the most common defect in the depositions formed by a pulsed-laser input and wire feed, particularly for the ladder-block structures.

Figure 16 illustrates the origin of incomplete fusion defects generated in ladder block samples (the arrows show direction of filling up of the liquid metal). The incomplete fusion defect is prone to be produced by an overlap process between the nearby beads or layers in the deposition process. Since the top surface of each layer of ladder blocks always fluctuates, the liquid metal has difficulty in filling up an uneven surface in a very short solidification time.

Moreover, in the pulsed laser and wire-based deposition processes, the molten pool is only 2–3 times greater than the diameter of a fine wire. In such a case, laser energy will be largely reflected or absorbed by the wire. Consequently, the metal wire may not sufficiently melt to form a stable metallurgical combination with the droplet. Furthermore, under an extremely fast solidification process, the wire feed speed is also limited. The wire feed speed must be adjusted to suit a stable deposition process.
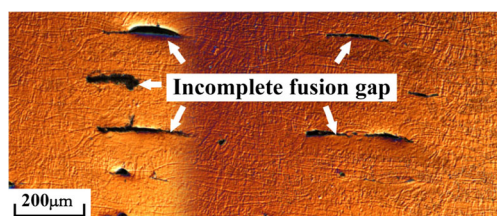

Fig. 15 Typical incomplete fusion defects in pulsed laser and wire feed depositions

4 Discussion

4.1 Formation and microhardness of the microstructural morphology

In the melting and solidification process of laser deposition, the formation of microstructures depends on the thermal history of the deposited metal. In pulsed laser deposition with a metal wire, the formation of a molten pool is also pulsed. The duration time of a pulsed laser input is 4 ms with 3 Hz pulsed frequency, which indicates that the heating input process is only 4 ms and the balance 329 ms is for the solidification and cooling processes in an overall single-pulsed process.

Figure 17 shows the typical history of the highest temperature of the molten pool (the average temperature for the central region of the molten pool) recorded by infrared thermography during the pulsed laser deposition process. According to the database of FLIR Systems Inc., the emissivity in this experiment was set to 0.28 (773–1773 K, 304 stainless steel, polished). The value recorded in the low-temperature region had a significant error, which is not discussed in this paper.

Four characteristic points are marked in a typical pulsed laser beam (Fig. 17a). Under the effect of thermal radiation by the photo-plasma and metal vapor, a very high peak temperature emerges in the beginning of the pulsed process (point 1). After 4 ms of the heating process (point 0 to 2), the solidification process starts. The molten pool is completely cooled down to an unmeasured temperature during this time, which is shown in Fig. 17b. The liquidus and solidus temperatures are evaluated to be 1723 and 1663 K, respectively, for austenite stainless steel according to a previous study by Li et al. [38]. On this basis, the cooling rate in the solidification process can be estimated as the temperature gradient from points 2 to 3, which is 1.7×10^5 K/s. Since an approximate value of emissivity was used, while no exact emissivity value in the totally same conditions of this experiment was known, the measured temperature gradient was only used for a reference of its magnitude.

According to the previous work of Katayama et al. [39], the relationship between the primary dendritic arm spacing and cooling rate for austenite stainless steel is given by Eq. 2:

$$d = 80\dot{T}^{-0.33} \tag{2}$$

where $\dot{T}$ is the cooling rate and d is the primary dendritic arm spacing. When $\dot{T}$ = 1.7×10^5 K/s, the primary dendritic arm spacing is 1.5 μm.

In addition, for the welding process with a continuous energy input, the cooling rate of the central line of the molten pool can be estimated by the Rosenthal solution (Eq. 3) [40]:

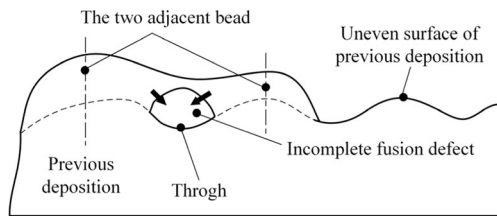$$\frac{dT}{dt} = -2\pi k \frac{v}{\alpha Q} (T - T_0)^2 \tag{3}$$

Fig. 16 Origin of incomplete fusion defect generated in ladder block samples

where dT/dt is the cooling rate, k is the thermal conductivity, v is the scanning velocity, α is the absorption rates of the energy input, Q is the energy input, T is the liquid-phase temperature, and T_0 is the environment temperature.

For the laser deposition process based on a continuous energy input, the cooling rate in the central line of the molten pool can be approximately estimated to be 10^3 K/s via Eq. 2 [32]. This estimated value is about 100 times smaller than the cooling rate measured in this experiment. Consequently, an extremely fine microstructure is formed with the process used in this study. In addition, the slower cooling rate corresponds to a larger heat accumulation, which is a prominent characteristic in the continuous energy-based deposition process. However, when pulsed energy is used, the heat will not be over accumulated in the deposition on rapid solidification, and a homogeneous microstructure morphology is produced in the direction of the deposition under a more even initial thermal condition [13, 32].

Furthermore, the micro hardness test of the thin wall samples is performed for elucidating the relationship between the different grain morphologies and micro mechanical properties. Because of the similar distribution regulation of microstructure morphologies in the different layer samples, only sample S5 was taken as example in this work. Figure 18 shows the microhardness values of different positions in section X of S5. The arrows perform the decreasing tendency of micro hardness from the interior to the surface. The measurement is in accordance with GB/T4340.1-2009 (standard of China), of which the errors in measured values are limited within 6% [41]. The average microhardness of the rolled austenite stainless steel substrate is 200 $HV_{0.2}$ (position 4). In addition to the surface of the deposition, microhardness in the middle position reaches between 230 and 267 $HV_{0.2}$ (position 3), while the microhardness value is 208–213 $HV_{0.2}$ (position 1–2) at the surface position, which is also higher than that in the substrate.

Combined with the observation results of grain morphology, it is found that microhardness in the surface positions is lower than that in the middle positions, while the grain size in the surface positions exhibits an opposite trend. Considering that the mixture of equiaxed grains and columnar grains along the scanning directions are observed in the top surface, it indicates that the different microstructure morphologies in local positions result in different micro hardness values. With the process used in this experiment, the average micro hardness is about 1.25 times as that of the cold rolling substrate made of austenite stainless steel. The special microstructure found in the surface results in a lower micro hardness, which is considered to be a valuable feature for the following study of surface subtractive machining process.

Fig. 17 Typical history of the highest temperature of the molten pool **a** under a single-pulsed laser beam and **b** under ten consecutive pulsed-laser beams
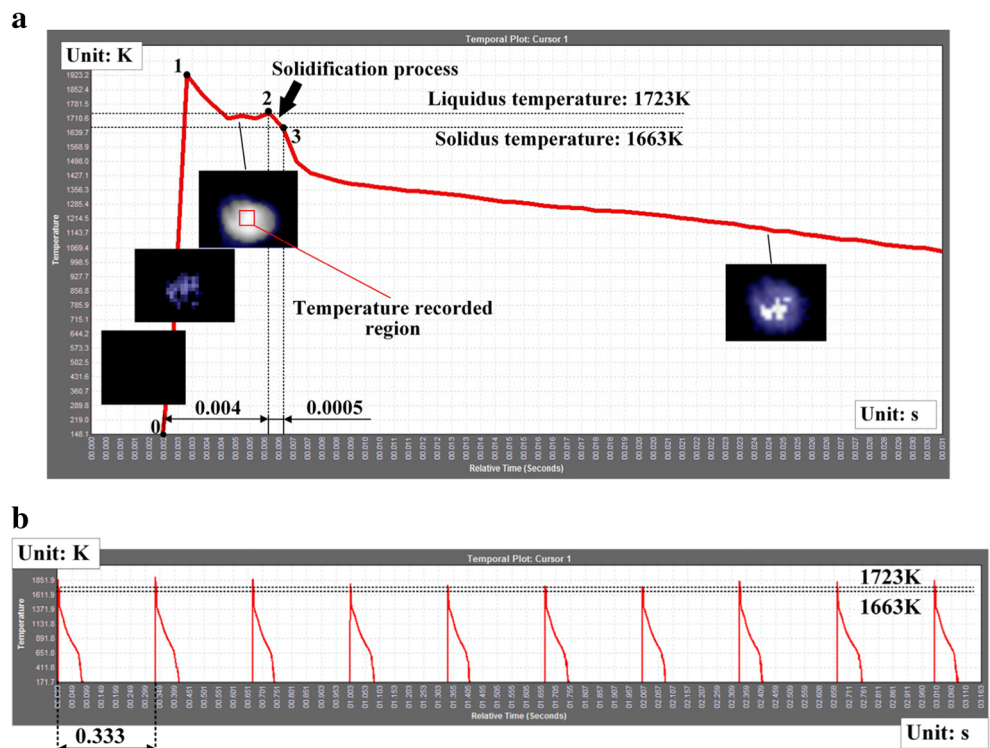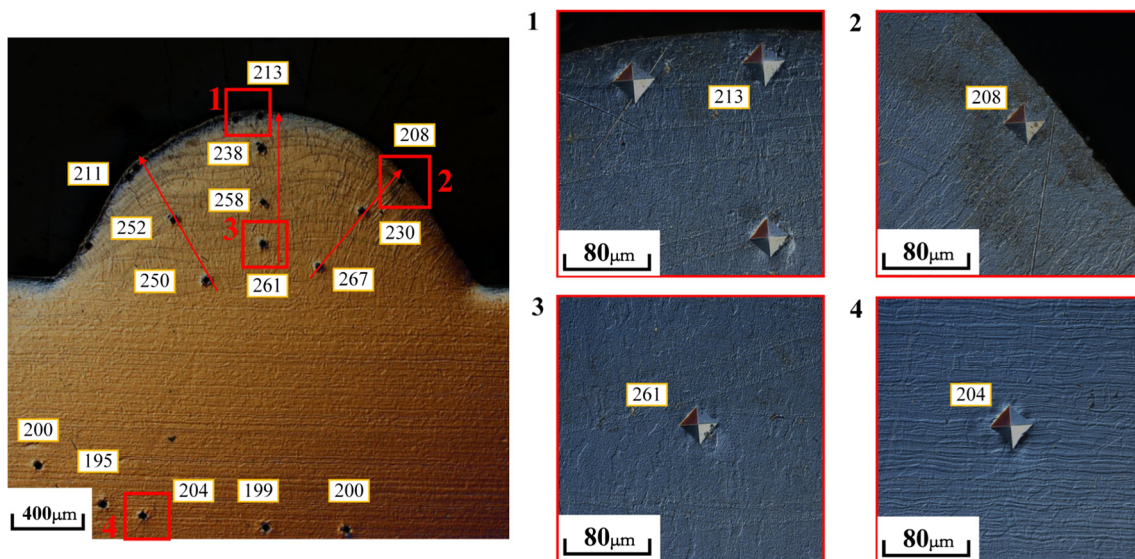
Fig. 18 Micro hardness values at different positions in section X of S5 (HV$_{0.2}$)

4.2 Mechanism of microstructural evolution

It is found that microstructures always vary with the different shapes of molten pools. Mostly, the shapes of molten pools represent the initial geometric conditions of nucleation and the heat effect. Therefore, if the shape of each molten pool is changed during the deposition process, the formation of microstructure will change concomitantly.

Figure 19 shows the different droplet transfers in the thin wall and ladder block processing (The arrows show the cooling direction in a molten pool). Because of the molten pool boundary from an adjacent bead, the liquid bridge in the ladder block deposition processing is also asymmetric, which induces the versatile grain growth direction in this position. A cooling direction that points to an adjacent bead being produced and more types of grain morphologies are formed under this basis.

The microstructure-evolution phenomenon is particularly clearly visible in thin wall depositions. Figure 20 shows the profiles of the top molten pools of each thin wall sample. (The
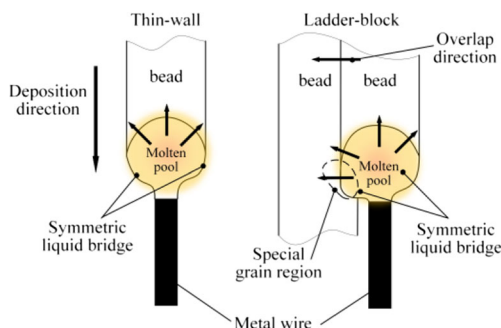

Fig. 19 Effect of the droplet transfer method on the thin wall and ladder block depositions

profiles are delineated from Fig. 7). Because of the effects of pulsed laser, several fusion lines are seen within the one-layer deposition. The fusion lines that are present throughout the entire width direction of section X can be regarded as the boundaries between adjacent layers. (The arrows show the grain-growth direction in this molten pool.) In the beginning of the thin wall deposition, the outer contour of section X presents a continuous curve shape, which indicates that the top molten pool almost covers the whole surface of depositions. Consequently, columnar grains grow on both sides of the deposition gradually (Fig. 20). With increasing deposited layers, the curvature of the top surface decreases gradually. In this study, the shape of the top surface starts to become almost horizontal in S13, and the outlines of the top and side surfaces are completely separated. In this time, the base of the molten pool was almost unchanged, and the shape of the molten pool became stable. Consequently, the microstructure morphology does not vary with the deposition process anymore (Fig. 20).

Nevertheless, the shape of the molten pool is actually more stable in the ladder block deposition than in the thin wall deposition, which is due to the effect of the overlap process. On the one hand, it makes the top surface of the ladder blocks smoother than that in the thin wall, which is an advantage condition for a stable deposition process. On the other hand, due to the limitation caused by the side boundary of the adjacent bead, space for the liquid metal flow will decrease. Consequently, there is no variation in the microstructures in the same positions of different ladder block samples.

In addition, the microstructures in the previous deposition are also changed even without the remelting process. Elements such as C, Cr, and Ni, are dissolved by the solid solution and reprecipitated during the recrystallization process, which is along the normal directions of the new fusion lines. Therefore,

Fig. 20 Profile of the top molten pool for thin-wall samples. The *arrows* indicate the grain growth direction in this molten pool
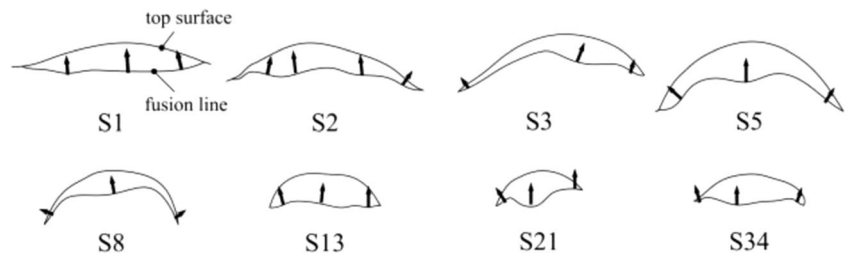
even at the same position, the microstructures in the depositions of different layer number samples of the thin wall are different. The elongated columnar grains that grow epitaxially by a similar extent will dominate in the deposition ultimately.

5 Conclusion

In this paper, the microstructure morphology and evolution of pulsed laser deposition with a metal wire were studied. A set of thin wall and ladder block samples were deposited. The material of both the substrate and metal wire was SUS304 austenite stainless steel. The following conclusions can be made from this study:

1. The microstructure is homogeneous in all the deposited samples due to the small heat accumulation under the pulsed laser input. Furthermore, for the thin wall, the columnar grains that are normal to the substrate, with a growth tendency to the surface and scanning direction, dominate the deposition. The boundary between the deposition bottom and substrate is quite clear. The mixture of columnar grains along the scanning direction and equiaxed grains is observed in the surface layer. For the ladder block, the columnar grains are observed along multiple growth directions. The boundary of the deposition bottom and substrate is unclear with many interlaced fusion lines. Several different grain morphologies are observed in the first 2–3 layers' depositions, particularly in the top surface. All the irregular grains become more directional with increasing number of deposited layers.

2. The grain size of deposited samples is extremely fine (typically less than 1.5 μm) due to the extremely fast cooling rate of each molten pool under millisecond pulsed laser (a magnitude of 10^5 K/s).

3. The micro hardness of the middle positions is larger than that of the surface positions in thin wall samples. Additionally, the microhardness in pulsed laser deposition is universally higher than that in the 304 cold rolling metal substrate.

4. The microstructures of thin wall sample evolve with the addition of the deposited layers, which is caused by the variation of molten pool shape.

Since the shape of the molten pool changes clearly with the deposition process, the nucleation position in the remelting region changes synchronously and the recrystallization in the HAZ will be along new cooling directions.

References

1. Arcella FG, Froes FH (2000) Producing titanium aerospace components from powder using laser forming. JOM 52(5):28–30

2. Cheah CM, Chua CK, Lee CW, Feng C, Totong K (2005) Rapid prototyping and tooling techniques: a review of applications for rapid investment casting. Int J Adv Manuf Technol 25(3–4):308–320

3. Wang HM (2014) Materials' fundamental issues of laser additive manufacturing for high-performance large metallic component[J]. Acta Aeronaut et Astronaut Sin 35(10):1690–2698

4. Levy GN, Schindel R, Kruth JP (2003) Rapid manufacturing and rapid tooling with layer manufacturing (LM) technologies, state of the art and future perspectives. CIRP Ann Manuf Technol 52:589–609

5. Ma M, Wang Z, Wang D, Zeng X (2013) Control of shape and performance for direct laser fabrication of precision large-scale metal parts with 316L stainless steel. Opt Laser Technol 2013(45):209–216

6. Kamath C, El-dasher B, Gallegos GF, King WE, Sisto A (2014) Density of additively-manufactured, 316L SS parts using laser powder-bed fusion at powers up to 400 W. Int J Adv Manuf Technol 74(1–4):65–78

7. Rombouts M, Kruth JP, Froyen L, Mercelis P (2006) Fundamentals of selective laser melting of alloyed steel powders. CIRP Ann Manuf Technol 55(1):187–192

8. Cherry JA, Davies HM, Mehmood S, Lavery NP, Brown SGR, Sienz J (2015) Investigation into the effect of process parameters on microstructural and physical properties of 316L stainless steel parts by selective laser melting. Int J Adv Manuf Technol 76(5–8):869–879

9. Lu SL, Tang HP, Ning YP, Liu N, StJohn DH, Qian M (2015) Microstructure and mechanical properties of long Ti-6Al-4V rods additively manufactured by selective electron beam melting out of a deep powder bed and the effect of subsequent hot isostatic pressing. Metall Mater Trans A 46(9):3824–3834

10. Wu MW, Lai PH (2016) The positive effect of hot isostatic pressing on improving the anisotropies of bending and impact properties in selective laser melted Ti-6Al-4V alloy. Mater Sci Eng A 2016(658):429–438

11. Vrancken B, Thijs L, Kruth JP, Humbeeck JV (2012) Heat treatment of Ti6Al4V produced by selective laser melting: microstructure and mechanical properties. J Alloys Compd 2012(541):177–185

12. Tammas-Williams S, Withers PJ, Todd I, Prangnell PB (2016) The effectiveness of hot isostatic pressing for closing porosity in titanium parts manufactured by selective electron beam melting. Metall Mater Trans A 47(5):1939–1946

13. Ding D, Pan Z, Cuiuri D, Li H (2015) Wire-feed additive manufacturing of metal components: technologies, developments and future interests. Int J Adv Manuf Technol 81(1–4):465–481

14. Wang F, Williams S, Colegrove P et al (2013) Microstructure and mechanical properties of wire and arc additive manufactured Ti-6Al-4V. Metall Mater Trans A 44(2):968–977

15. Wang F, Williams S, Rush M (2011) Morphology investigation on direct current pulsed gas tungsten arc welded additive layer manufactured Ti6Al4V alloy. Int J Adv Manuf Technol 57(5–8):597–603

16. Brandl E, Schoberth A, Leyens C (2012) Morphology, microstructure, and hardness of titanium (Ti-6Al-4V) blocks deposited by wire-feed additive layer manufacturing (ALM). Mater Sci Eng A 2012(532):295–307

17. Biamino S, Penna A, Ackelid U et al (2011) Electron beam melting of Ti–48Al–2Cr–2Nb alloy: microstructure and mechanical properties investigation. Intermetallics 19(6):776–781

18. Dicks R, Wang F, Wu X (2009) The manufacture of a niobium/niobium-silicide-based alloy using direct laser fabrication,[J]. J Mater Process Technol 209(4):1752–1757

19. Bird R K,Atherton T S (2010) Effect of orientation on tensile properties of Inconel 718 block fabricated with electron beam freeform fabrication (EBF3)

20. Zhang YN, Cao X, Wanjara P (2013) Microstructure and hardness of fiber laser deposited Inconel 718 using filler wire. Int J Adv Manuf Technol 69(9–12):2569–2581

21. Ekrami Y, Forth S C, Waid M C (2011) Characterization of electron beam free-form fabricated 2219 aluminum and 316 stainless steel

22. Nie Z, Wang G, McGuffin-Cawley JD et al (2016) Experimental study and modeling of H13 steel deposition using laser hot-wire additive manufacturing. J Mater Process Technol 2016(235):171–186

23. Taminger K,Hafley R A (2003) Electron beam freeform fabrication: a rapid metal deposition process

24. Ding D, Pan Z, van Duin S, Li H, Chen S (2016) Fabricating superior NiAl bronze components through wire arc additive manufacturing. Materials (Basel) 9(8):652

25. Frazier WE (2014) Metal additive manufacturing: a review. J Mater Eng Perform 23(6):1917–1928

26. Farshidianfar MH, Khajepour A, Gerlich AP (2016) Effect of real-time cooling rate on microstructure in laser additive manufacturing. J Mater Process Technol 2016(231):468–478

27. Huang C, Lin X, Li F, Cao J, Huang W (2016) Effects of cooling condition on microstructure and mechanical properties in laser rapid forming. Int J Adv Manuf Technol 82(5–8):1269–1279

28. Yang M, Qi B, Cong B et al (2013) Effect of pulse frequency on microstructure and properties of Ti-6Al-4V by ultrahigh-frequency pulse gas tungsten arc welding. Int J Adv Manuf Technol 68(1–4):19–31

29. Tsai HL, Zhou J, Lehnhoff TF (2006) Investigation of transport phenomena and defect formation in pulsed laser keyhole welding of zinc-coated steels. J Phys D Appl Phys 39(24):5338

30. Morgan R, Sutcliffe CJ, O'Neill W (2001) Experimental investigation of nanosecond pulsed Nd:YAG laser re-melted pre-placed powder beds. Rapid Prototyp J 7(3):159–172

31. Morgan R, Papworth A, Sutcliffe C, et al (2001) Direct metal laser re-melting (DMLR) of 316L stainless steel powder part 1: analysis of thin wall structures. // solid freeform fabrication symposium: 276-282

32. Abe F, Osakada K, Shiomi M et al (2001) The manufacturing of hard tools from metallic powders by selective laser melting. J Mater Process Technol 111(1):210–213

33. Nassar AR, Reutzel EW (2015) Additive manufacturing of Ti-6Al-4V using a pulsed laser beam. Metall Mater Trans A 46(6):2781–2789

34. Ye Z, Zhang Z, Jin X, Xiao M, Su J (2016) Study of hybrid additive manufacturing based on pulse laser wire depositing and milling. Int J Adv Manuf Technol, 1-12

35. Kobryn PA, Moore EH, Semiatin SL (2000) The effect of laser power and traverse speed on microstructure, porosity, and build height in laser-deposited Ti-6Al-4V. Scr Mater 43(4):299–305

36. Kelly SM, Kampe SL (2004) Microstructural evolution in laser-deposited multilayer Ti-6Al-4V builds: part I. Microstructural characterization. Metall Mater Trans A 35(6):1861–1867

37. Kelly SM, Kampe SL (2004) Microstructural evolution in laser-deposited multilayer Ti-6Al-4V builds: part II. Thermal modeling. Metall Mater Trans A 35(6):1869–1879

38. Li JY, Sugiyama S, Yanagimoto J (2005) Microstructural evolution and flow stress of semi-solid type 304 stainless steel. J Mater Process Technol 161(3):396–406

39. Katayama S, Matsunawa A (1985) Solidification microstructure of laser welded stainless steels. Laser Institute of America 1985:60–67

40. Rosenthal D (1946) The theory of moving sources of heat and its ap-plication to metal treatments. // ASME

41. GB/T4340.1–2009 (2009) [S], Standards Press of China, Beijing